Title:

Thermomechanical Analysis and Modeling of Involute-Shaped Fuel Plates Using the Cheverton–Kelley Experiments for the High Flux Isotope Reactor

Authors:

Marta Sitek[1], Argonne National Laboratory, 9700 S Cass Avenue, Lemont, 60439, IL, USA, msitek@anl.gov

Kaltrina Shehu, Forschungs-Neutronenquelle Heinz Maier-Leibnitz (FRM II), Technische Universität München, Lichtenbergstraße 1, Garching, 85748, Germany, kaltrina.shehu@frm2.tum.de

Prashant Jain, Oak Ridge National Laboratory, 1 Bethel Valley Road, Oak Ridge, 37830, TN, USA, jainpk@ornl.gov

Aurélien Bergeron, Argonne National Laboratory, 9700 S Cass Avenue, Lemont, 60439, IL, USA, abergeron@anl.gov

Jeremy Licht, Argonne National Laboratory, 9700 S Cass Avenue, Lemont, 60439, IL, USA, jlicht@anl.gov

Christian Reiter, Forschungs-Neutronenquelle Heinz Maier-Leibnitz (FRM II), Technische Universität München, Lichtenbergstraße 1, Garching, 85748, Germany, christian.reiter@frm2.tum.de

Abstract:

Three research reactors with involute-shaped fuel plates are pursuing conversion from highly-enriched uranium to low-enriched uranium fuel. Various core design and safety evaluation studies are essential to assess the feasibility of the conversion. The use of 3D computational multiphysics codes is being explored in these analyses and therefore they must undergo a thorough evaluation and quality assurance process due to their potential impact on nuclear safety. In the present study, the Cheverton and Kelley physical tests performed in the late 1960s to investigate the deflections of HFIR's outer plate under uniform pressure and temperature fields are simulated by employing commercially-available computational codes, with the goals to (1) verify and validate the models and numerical solvers implemented in the codes for thermomechanical analysis of involute reactor plates and (2) to develop a benchmark computational test to evaluate future versions of existing software or newly developed computational codes. The results of the simulations showed good agreement with each other as well as against the Cheverton–Kelley experimental data. Some minor deviations were observed for a few multiphysics cases and their potential origins and impact on the analysis results is investigated in the paper. The validated models increase the confidence in using Multiphysics codes to evaluate existing or new LEU designs.

Keywords:

thermomechanical modeling, high performance research reactor, LEU conversion, verification and validation, involute plates, multiphysics

[1] Corresponding author/technical contact

1. Introduction

The High Flux Isotope Reactor (HFIR) [1] in Oak Ridge, Tennessee, USA, the High Flux Reactor (RHF) [2] in Grenoble, France, and the Research Neutron Source Heinz Maier-Leibnitz (FRM II) [3] in Garching, Germany, are in a unique class of research reactors that use involute-shaped fuel plates to form their cores. The cores in these three reactors are being converted from highly enriched uranium (HEU) to low-enriched uranium (LEU) fuel plates. These conversions will support global nonproliferation objectives to minimize the use of weapons-grade HEU materials around the world.

Analysts from these reactors are performing various core design and safety evaluation studies to assess the feasibility of conversion to LEU fuel. The LEU conversions may require substantial changes to reactor fuel and core designs to preserve performance and mission relevance or meet thermal safety margin requirements. Therefore, thorough evaluations of the new LEU plate and core designs to account for thermal, hydrodynamic, and mechanical analyses, become essential to the conversion process.

Advanced computational tools are being explored in these analyses instead of the traditional methods such as 1D or 2D codes. For many years, computational fluid dynamics (CFD) and computational structural mechanics (CSM) software have been widely used by engineers in other fields and have also gained popularity throughout the nuclear community.

Because of their nuclear safety impacts, new scientific tools to be used in reactor design and analyses must undergo a thorough evaluation and quality assurance process. Therefore, operators from the three reactors and Argonne National Laboratory formed the Involute Working Group (IWG) [4]. Their activities include (1) identifying CFD and CSM codes that can perform the required calculations, (2) gathering and evaluating existing data for benchmarking, verification, and validation of the solvers based on experimental data and code-to-code comparison, and (3) design of new experiments to support the conversion process.

HFIR, RHF, and FRM II rely on a specific curved shape of the fuel plate—the involute of a circle—in their annular core designs. Because of the unique involute shape, the fuel plates can be uniformly distributed inside the core annulus in the azimuthal direction to create a compact core. In this core assembly type, all the coolant channels are identical, with a constant thickness along the arc of the plate. However, some local deviations could occur because of manufacturing imperfections. All these fuel plates experience similar irradiation conditions, with some possible local azimuthal variations induced by the presence of safety or experimental components near the fuel elements. These fuel plates have a large length-to-thickness aspect ratio: their length is of an order of magnitude of one meter, and the thickness is of an order of magnitude of one millimeter.

The imperfections mentioned above could lead to hydrodynamic and thermal loads causing excessive deformation of the slender structures. To keep the fuel plates stationary, they are attached longitudinally to an inner and outer cylindrical component, commonly called the *inner and outer side plates*, as shown in Fig. 1 from HFIR. Both edges of a fuel plate are inserted into their corresponding side plate grooves and are then welded together at specific intervals, usually at one weld for every 25.4 mm (1 inch) of the plate length. These weld attachments play a crucial role in keeping the fuel plates structurally stable and geometrically consistent under the high flow rates, temperatures, pressure differentials, and induced stress conditions present in high-performance research reactors. During normal operation, the plates experience thermal expansion and fluid-structural interaction and may undergo local elastic and plastic deformations. If a fuel plate is not correctly seated in the core because of a manufacturing or assembly defect, these dynamic forces could trigger a local or cascaded weld failure in the core. This could lead to a large plate and channel deformation in the core, which, depending on how the transient unfolds, could jeopardize the structural integrity of the fuel plates, and could lead to overheating of the core. Therefore, the sensitivity of the fuel plates' structural integrity to various parameters must be explored.

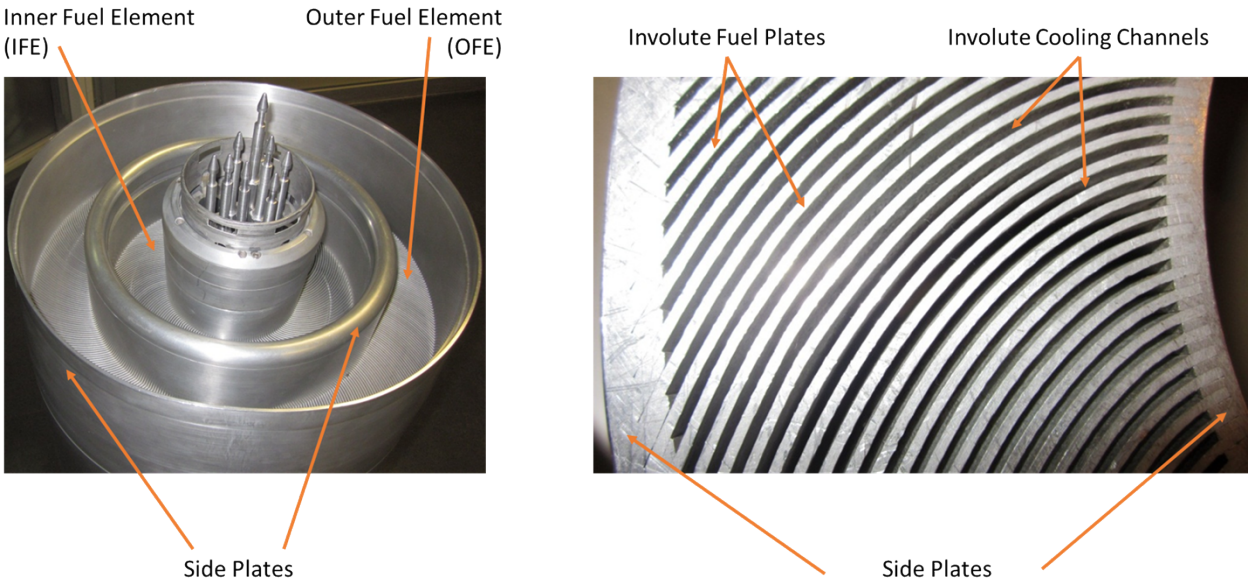

Fig. 1. Inner and outer fuel elements of HFIR (left), and a detailed view of involute fuel plates, cooling channels, and side plates (right).

In the late 1960s, Cheverton and Kelley [5] performed a series of experiments to investigate the pressure- and temperature-induced deflections of HFIR's outer plate as part of the HFIR research program. In the present study, the Cheverton and Kelley thermomechanical experiments are simulated by employing three commercially-available computational codes: ANSYS Mechanical [6], COMSOL Multiphysics [7], and Simcenter STAR-CCM+ [8].

One of the key objectives of this effort is to elevate the Cheverton–Kelley tests as an international benchmark for the involute-plate–fueled research reactors. This paper highlights major details of the experiments—including set-up dimensions, material choices and properties, and test conditions—to ensure reproducibility of the results within the experimental or computational accuracy margins.

Other goals are to verify and validate the models and numerical solvers implemented in the three codes for thermomechanical analysis of involute reactor plates and to develop a benchmark computational test to evaluate future versions of existing software or newly developed computational codes. According to ASME's Standard for Verification and Validation in Computational Solid Mechanics [9], "verification is the process of determining that a computational model accurately represents the underlying mathematical model and its solution," whereas "validation is the process of determining the degree to which the model is an accurate representation of corresponding physical experiments from the perspective of the intended uses of the model." In this study, verification is based on a code-to-code comparison of numerical solutions, and validation is based on comparing simulation output to experimental measurements. The results from the three codes are compared to each other and to the experimental data for a set of physical tests. When developing the computational models, some simplifying assumptions were made so that other researchers could reproduce the results. A few best-estimate approximations were also made if pertinent information was missing or not readily available. All details of the computational process are provided in the sections below.

2. Cheverton–Kelley Experiments

The HFIR core is made of two concentric fuel elements, as shown in Fig. 1. The side-plates form three annuli with different radii. The fuel plates are installed within grooves cut in the side plates, spot-welded to the side plates in 24 locations, and uniformly distributed along the lengths of the plates. Both short ends

of the plates are constrained with combs to prevent deflections further. The inner plates have a larger span, and because the generating circle has a smaller radius, they are more curved than the outer plates. The outer plates are flatter but shorter in span than the inner plates.

Cheverton and Kelley performed thermomechanical experiments on an involute-shaped fuel plate mockup with the same dimensions as the HFIR outer fuel plate under various thermal and pressure loads and differing constraints. Outer plates were tested because they have a larger curvature radius and may be more susceptible to buckling than the inner plates. The goal was to investigate its deflections and its tendency to buckle under extreme loads.

The experiments were conducted under simplified conditions compared to the actual conditions of the operating reactor core. In the reactor, the fuel and side plates may experience slightly nonuniform temperature and pressure distribution resulting from a variation in power distribution throughout the core. They may also experience a pressure differential across two adjacent channels caused by the coolant flowing in the parallel channels, which may have shape imperfections. The experiments subjected a single plate to thermal loads with a uniform temperature up to 316 °C and applied a range of uniform pressure loads up to 207 kPa to the concave surface of the plate at a room temperature of 27 °C in combination with a thermal load. The combs were omitted from the physical tests, but the degree of end restraint was varied in such a way as to give some indication of the effect. The weld attachments were represented by adding 24 tabs on each long side of the plate. The tabs were of two widths, 6.35 and 3.18 mm, to study the impact of varying thickness of the weld attachments.

The experiments selected for computational modeling in this effort analyzed various loading and displacement constraints. In four of the tests, a pressure load was applied to the concave surface of the plate, and varied constraints were applied to the tabs and the involute. In the subsequent three tests, a temperature load was applied to the model, and the material properties of the plate and the mounting base configuration changed. A combination of pressure and temperature loads was also considered.

Cheverton and Kelley used differential transformers to measure the plates' deflections. The transformers were mounted on a bridge and spaced uniformly along the arc length in seven locations. The styluses were normal to the true involute curve at their theoretical contact points. The positions of the styluses along the involute arc length were: (1) 3.175 mm, (2) 14.605 mm, (3) 26.035 mm, (4) 37.465 mm, (5) 48.895 mm, (6) 60.325 mm, (7) 71.755 mm. The bridge was mounted on the track to take measurements at various axial locations. To accommodate the transformers used in the tests, the accuracy at which the displacements of points on the plate could be determined was established as 0.0254 mm. The limiting temperature for a sustained operation of the styluses was approximately 204 °C, which was the required maximum temperature in most tests. A temperature of 316 °C was reached only in the final test.

Some data scatter was noticed in the measurements. For tests where the degree of end fixation was a variable, the actual degree of partial end restraint achieved in each test was not accurately established. Also, the variation in the initial fabricated shape of the plate, as well as the changes in the shape caused by installation in the base, were observed during the experiments. The deviation from the involute reached up to 0.3 mm in the reported data. The non-uniformity of the end and side attachments may have also influenced the measurement results.

Three physical tests were performed on fuel plates using the same constraint and load conditions to estimate the uncertainty of the deflection measurements. On average, the data vary ±6%, with a maximum absolute difference of 11% compared to the mean. It is important to note that in most cases, the maximum deflections of the fuel plates reach a fraction of one millimeter, which is less than the plate thickness.

3. Solvers Used in the Computations

The software versions used in this study were ANSYS Mechanical v. 22.R1, COMSOL Multiphysics v. 6.0.0.318, and Simcenter STAR-CCM+ v. 16.04. These codes use the finite element method (FEM) for solving thermo-mechanical problems.

The FEM was implemented in ANSYS in the 1990s and followed the pure displacement formulation, as well as the mixed displacement-pressure formulation [6]. The hexahedra finite elements, called SOLID185, which have eight nodes and linear shape functions, were used in the current calculations. The enhanced strain formulation [10], [11] is added to SOLID185 for linear and nonlinear analysis, respectively, to overcome locking. Direct and iterative solvers are available in ANSYS, but the sparse direct solver was used throughout this study. More details on the implementation can be found in the ANSYS APDL Theory Reference [6].

COMSOL Multiphysics [7] is a cross-platform FEM analysis, solver, and multiphysics simulation software. It allows for the modeling and simulation of physics-based coupled systems of partial differential equations. The Cheverton–Kelley thermomechanical problem is modeled using two physics modules of COMSOL—Solid Mechanics, and Heat Transfer in Solids—which are coupled to model thermal expansion physics. The quadratic Lagrange shape functions are used to model the displacement field, whereas linear shape functions are used to model temperatures. In addition, the FEM models are solved without including geometric nonlinearities. Depending on the simulated case, the models rely on segregated and fully coupled solvers using direct PARDISO, or MUMPS approaches.

The structural solver in Simcenter STAR-CCM+ was initially developed as a finite volume solver, and then the FEM was introduced more recently. Implementation of FEM follows the Lagrangian displacement finite element formulation [12]. Hexahedral finite elements with eight nodes and linear shape functions, HEX8, were selected for this study. The linear shape functions used in the finite element formulation approximate the topology of the continuum, as well as the displacement field. The strain-displacement relationship of the HEX8 finite element is enriched with so-called "bubble functions" whose derivation is based on the same references [10] as in the case of the SOLID185 finite elements from ANSYS. The original formulation was later extended to geometrically nonlinear finite elasticity and plasticity [13], [11]. The current study tested the nonlinear geometry solver, and the results were compared to those obtained with the linear geometry solver. The material model adopted in the simulations is linear elastic with constant properties. The elastic-plastic material model was employed in the previous phase of the study [16]. The sparse direct solver with the backward Euler integration method was used to solve the matrix equations. For more details on implementation in STAR-CCM+, refer to the user's manual [8].

4. Overview of the Computational Models

4.1. Geometry of the Model

The model geometry is developed in SolidWorks v.2020 [14] and imported to the three computational programs to perform the CSM simulations. Detailed drawings of the involute plate's geometry, including tabs, are available in Cheverton and Kelley's report. A few drawings and photos of the mounting base are provided, but they do not cover all details necessary to reproduce its geometry accurately. For this reason, simplifying assumptions were made, and the final model may be slightly different from the assembly Cheverton and Kelley used in their experiments. Additionally, the experimental assembly included multiple bolts and screws, as well as other attachments not included in the model. The differences between the computational geometry of the model and the physical assembly may be responsible for some discrepancies in the predicted displacements presented in the following sections. The full recreated geometry is shown in Fig. 2. Note that only the plate and the base with endplates are used for computations; the full model was developed for presentation purposes only. Fig. 3 shows drawings of the involute fuel plate with tabs measuring (a) 6.35 mm and (b) 3.18 mm wide.

(a) (b)

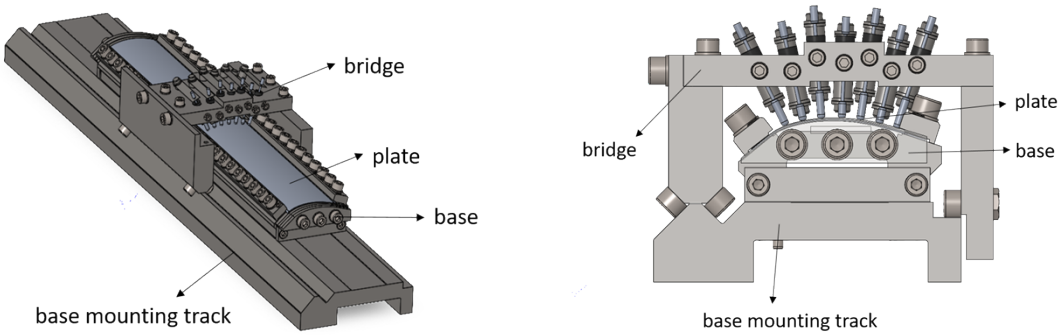

Fig. 2. Model geometry: perspective view (a), and front view of the experimental assembly (b).

(a)

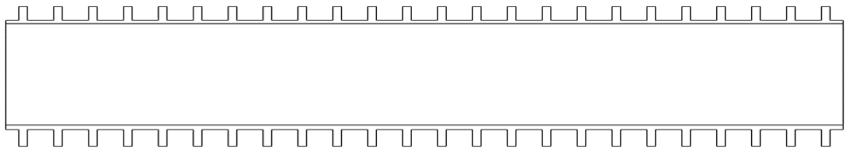

(b)

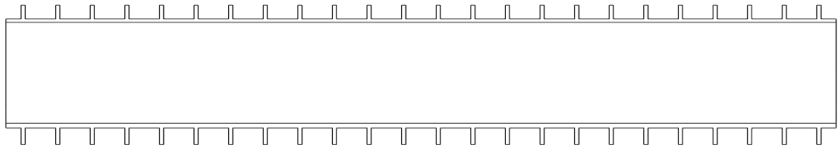

Fig. 3. Top view of fuel plate models with tabs measuring 6.35 mm (a) and 3.18 mm (b) wide.

4.1. Material Models

The Cheverton–Kelley experiments were performed on two types of plates: (1) aluminum plates with a fuel core, and (2) pure sheet aluminum AA-6061-T0 plates. The report states that the deflections of the two types of plates were in good agreement under the same loads and constraints. Therefore, the involute plates were modeled without the fuel core to simplify the computational modeling efforts. This approach was tested in previous studies [15], [16] and proved to give good accuracy of results. The involute plate material was modeled as aluminum alloy AA-6061-T0 or aluminum with so-called "cold ends" made of carbon steel, depending on the case due to the presence of a 5-cm-long unfueled section on each end of the HFIR fuel plate. The base was assigned properties of Invar, carbon steel, and Monel, depending on the case. Cheverton and Kelley selected these metals because of their thermal expansion coefficients that vary from 1.3 μm/m K for Invar to 23.6 μm/m K for aluminum, allowing varying levels of deformation of the base under thermal load to be simulated. The endplates were made of aluminum alloy.

The material properties of the metals used in the physical tests were not given explicitly in Cheverton and Kelley's report. They reported that the response of the plate was elastic in most of the tests, and plastic flow at the attachments was only observed in a few cases. In an earlier study [15], it was assumed that the material model was isotropic linear elastic and that the material properties in the literature corresponded to those at a temperature of 27 °C. Jain et al. [16] expanded the analysis to include the material properties dependent on temperature, and the influence of an elastic-plastic material model on the deflection magnitude was

tested. It was found that if the plate response is within or close to the elastic range, then the computational results show an excellent accuracy compared to the physical tests. Even though an elastoplastic material model better represents the mechanical response, discrepancies occur when the loads are large enough to result in plastic flow. A sensitivity study performed to analyze the influence of small changes in elastic mechanical properties on plate deflections showed that the dependence is linear.

The analysis described herein adopted an isotropic linear elastic material model for all considered metals. This widely used model represents the behavior of metals in the elastic regime, making the model replicable and more straightforward. The material properties used in the study are based on data found in the report by Jain et al. [15] and are presented in Table 1.

Table 1

Material properties used in the computational models.

Material	Thermal expansion coefficient (μm/m K)	Thermal conductivity (W/m K)	Density (kg/m^3)	Specific heat capacity (J/kg K)	Modulus of elasticity (GPa)	Poisson's ratio (-)
AA-6061-T0	23.6	167.0	2,700	896	69	0.33
Carbon steel	12.9	47.4	7,850	477	203	0.29
Invar	1.3	10.15	8,050	515	141	0.30
Monel	13.9	21.8	8,800	427	169	0.295

4.2. Loads and Constraints

Ten cases were selected from the experiments to comprehensively evaluate the solvers, including various load, constraint, and material types. All selected cases were static with uniform pressure or temperature loads and constant displacement constraints. Detailed descriptions of the load and constraint conditions and the material models used in the simulations are presented in Table 2. The displacement constraints are marked in the figures with different colors for clarity.

This set of cases was selected to consider the separate effects of loads and constraints and to subsequently analyze their combined effects. Therefore, the cases considered in the study included only pressure load (Cases 0–4), only temperature load (Cases 5–9), and a combination of both (Case 10). Two models were proposed to solve the problem: a model of a single plate (Cases 0–5), and a model of a plate in a base (Cases 6–10). These models are described in the following sections.

Because of the uncertainty in the plate constraint conditions in the physical tests and the simplifications made in the geometry of the computational model, various displacement boundary conditions were tested previously [16]. It was found that the changes in boundary conditions had the greatest impact on plate deflections. Only the variants resulting in the most accurate responses are considered here.

4.2.1. Model of a Single Plate

It has been shown [16] that a plate model without the base can be used successfully in problems without thermal loads or when the increasing temperature does not result in significant deformation of the base compared to the plate deformation. The base is eliminated from the model, and instead, a condition of zero displacements is utilized on sections of the model. Table 2 presents the types of constraints considered in the study for the model of a single plate. This simplification saves computational time and resources, but it does not introduce significant errors to the solution in the considered cases. If a single-plate model is used to model problems with a significant base deformation, then the plate deflections are expected to be overestimated.

4.2.2. Model of a Plate in a Base

The base used in the experiments was built using carbon steel, Invar, and Monel to simulate the thermal expansion of the HFIR side plates that may occur in the reactor. These materials have different thermal expansion coefficients, as shown in Table 1, thus allowing for modeling a varying level of constraint applied to the plate under thermal loads. Additionally, steel plates were attached to the short ends of the base to partially constrain the deformation of the base. In the computational model, the bottom surfaces of the base, where the experimental base is in contact with the table, have been applied a zero normal displacement, allowing for movement in the horizontal plane but preventing vertical motion. To eliminate the rigid-body motion of the model, a small section of one of the endplates was constrained, and three components of the displacement vector were equal to zero. The location and size of this section were chosen so that it has the least possible influence on the overall deformation of the model.

The base was considered as a whole and was divided into two portions. The two bases used in the model, one solid (a) and the other divided into two parts (b), are depicted in Fig. 4. The gap between the two components of the split base was 2 mm wide, as shown in the figure. The division makes it possible for the two parts of the base to experience a relative motion. Under a temperature load, the base deforms according to its thermal expansion coefficient, and in turn, it displaces the tabs and deforms the plate.

The model of the plate in a base was constructed of separate parts: the base (as a whole or divided in two), two top bars, two endplates, and the involute plate with tabs. Contact interactions are implemented between the components. One type of contact assures the continuity of displacements between two surfaces, and another allows two surfaces to slide over each other without any movement in the direction normal to the surfaces or friction. The first contact type was used between the surfaces of the plate tabs and the base to model the condition in which the tabs were constrained in the base. In ANSYS and STAR-CCM+, this type of contact is called a *bonded interaction*, and in COMSOL is known as an *identity-pair boundary condition*. The contact second type was used to model the interaction between the tabs that are not attached to the base with the base, as well as the plate and the base, to eliminate the possibility of the two bodies intersecting each other when subjected to load. In ANSYS, this is called a *no-separation contact formulation*, and in STAR-CCM+, a small sliding frictionless interaction is used. Frictionless contact formulation is used based on its availability within the three codes. The implementation of the interaction behavior between two deformable bodies may differ from code to code, even if the naming convention suggests otherwise. Results of a comparative analysis between the codes are reported in the sections below, showing minor discrepancies between the models.

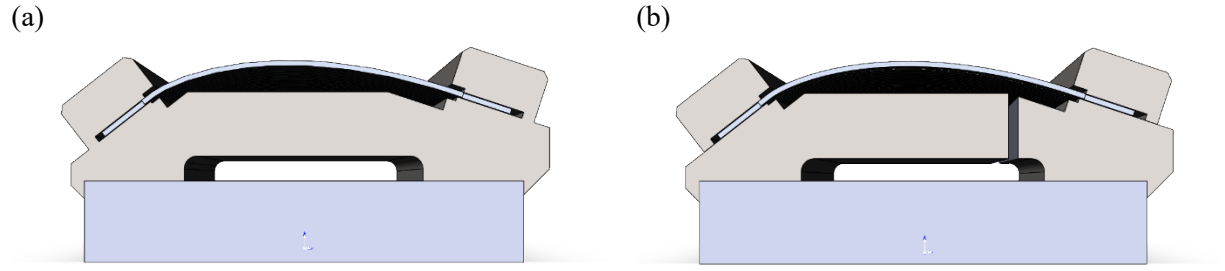

Fig. 4. Solid (a) and divided (b) base types modeled.

Table 2
Load and constraint conditions and materials used in the cases considered in the computational study. Magenta indicates displacements constrained in all three directions, green indicates a constraint in the normal direction, blue indicates a sliding contact, and yellow indicates a bonded contact.

Case number	Loads	Material properties	Constraints
Reference case C0	Uniform pressure load 207 kPa applied to the concave surface of the involute	Aluminum plate	Zero displacements on the side surfaces of the involute plate without tabs 
C1	Uniform pressure load applied to the concave surface of the involute and the straight side strips of the plate For each type of constraint, the load varies from 69 to 207 kPa		Zero displacements on the 6.35 mm wide tabs, thin strips along the long edges of the plate, and short ends of the plate 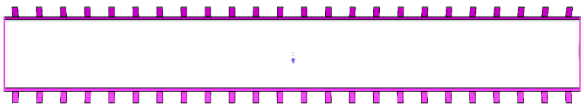
C2			Zero displacements on the 6.35 mm wide tabs and plate's short ends 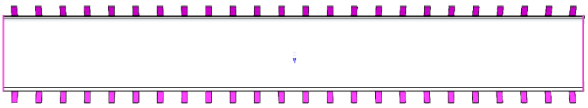
C3			Zero displacements on every other 6.35 mm wide tab and the plate's short ends 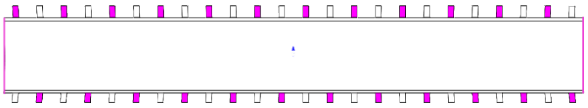
C4			Zero displacements on the 3.18 mm wide tabs and the plate's short ends 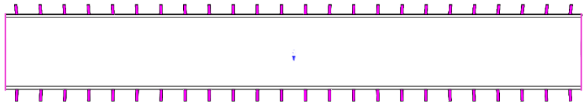
C5	Uniform temperature load of 204 °C, initial temperature of 27 °C	Aluminum plate	Zero displacements on the 6.35 mm wide tabs. 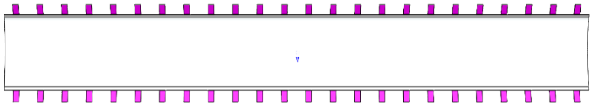
C6		Aluminum plate, solid Invar base	Zero displacements on a feature line on one of the end plates, zero normal displacements on the bottom surfaces of the base, and a bonded contact between the end plates and the base, and 6.35 mm wide tabs and the base
C7		Aluminum plate, split Invar base	
C8		Aluminum plate, split steel base	
C9		Aluminum and steel plate,	

Case number	Loads	Material properties	Constraints
		split Invar base	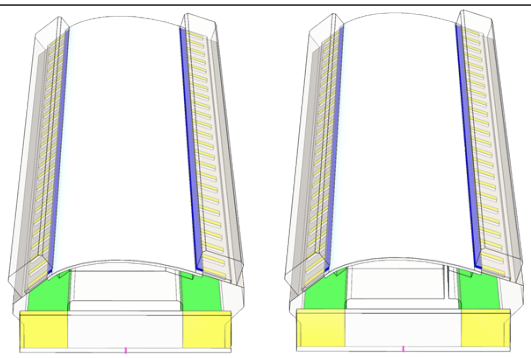
C10	Uniform pressure load equal to 207 kPa applied to the concave surface of the involute and the straight side strips of the plate Uniform temperature load of 204 °C, initial temperature 27 °C	Aluminum plate, solid Monel base	Zero displacements on a feature line on one of the end plates and on the short ends of the plate, zero normal displacements on the bottom surfaces of the base, and a bonded contact between the end plates and the base and 6.35 mm wide tabs and the base. 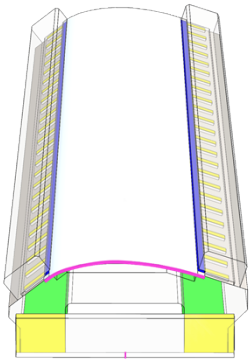

5. Mesh Sensitivity

A mesh sensitivity analysis was performed on a model of an involute plate with tabs measuring 6.35 mm wide, corresponding to Case C2. The surfaces of the plate's short ends, as well as the top and bottom surfaces of the tabs, were constrained. A uniform pressure load of 69 kPa was applied to the concave surface of the involute plate. The deflection of the convex surface that was perpendicular to the surface was monitored during the simulations.

Three mesh densities were considered in the analysis, referred to herein as coarse, medium, and fine meshes. In the coarse mesh, 2 × 50 × 400 linear finite elements were used in the thickness, span, and length directions, respectively. In the medium mesh, the number of finite elements was increased to 4 × 100 × 400 in the respective directions, and in the fine mesh, 8 × 200 × 400 finite elements were used. Fig. 5 presents views of the discretizations.

Initially, the mesh sensitivity analysis in all three software was performed with the use of finite elements with linear interpolation of displacements. However, the COMSOL model showed a significant difference in results compared to the other software and measurement data. Therefore, it was decided to repeat the analysis using the more-accurate quadratic Lagrangian finite elements.

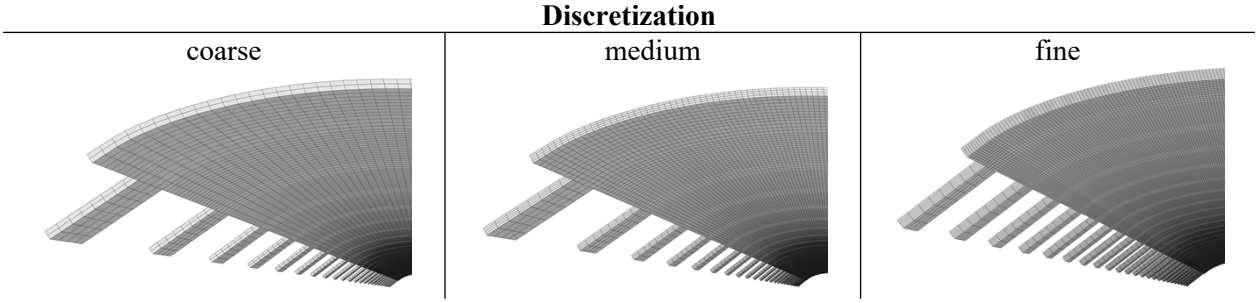

Fig. 5. Coarse, medium, and fine discretization density used in the mesh sensitivity analysis in ANSYS, COMSOL, and STAR-CCM+ with the use of linear finite elements.

The maximum and minimum displacement normal to the plate convex surface and the relative difference from the fine linear finite element mesh solution are presented in Table 3 for ANSYS, Table 4 for COMSOL, and Table 5 for STAR-CCM+. Fig. 6 shows the mid-length normal displacements that were obtained using the three codes. The differences in the minimum and maximum deflections of the midspan are low compared to those of the fine mesh solution.

For the medium mesh with linear finite elements in ANSYS and STAR-CCM+, the relative differences equal 1% and 2%, respectively, and 5% and 6% for the coarse mesh. Therefore, the medium mesh with linear finite elements was selected for further analysis with ANSYS and STAR-CCM+. The computations performed in COMSOL with linear finite elements resulted in a relative difference from the fine mesh solution of 40% for the coarse mesh and 10% for the medium mesh. In the coarse quadratic finite element mesh, $1 \times 25 \times 200$ quadratic elements were used in the thickness, span, and length directions, respectively. In the medium quadratic mesh, the number of quadratic elements was increased to $2 \times 50 \times 200$ in the respective directions, and in the fine quadratic mesh, $4 \times 100 \times 200$ quadratic elements were used. The mesh sensitivity results for the quadratic elements in COMSOL are provided in Table 6 and are plotted in Figure 6(d). The medium quadratic finite element mesh results in a good agreement with its fine mesh results; hence, a medium mesh was selected for further analysis. The solutions obtained from all three software with a medium density mesh are plotted in Fig. 7.

Table 3
Linear finite element mesh sensitivity analysis input and results for ANSYS.

Mesh type	Number of degrees of freedom	Displacement normal to the plate convex surface (mm)		Relative difference from the fine mesh solution	
		Maximum	Minimum	Maximum	Minimum
Coarse	1.89×10^5	0.057	-0.019	5%	6%
Medium	6.27×10^5	0.059	-0.020	1%	1%
Fine	21.7×10^5	0.060	-0.021	-	-

Table 4
Linear finite element mesh sensitivity analysis input and results for COMSOL.

Mesh type	Number of degrees of freedom	Displacement normal to the plate convex surface (mm)		Relative difference from the fine mesh solution	
		Maximum	Minimum	Maximum	Minimum
Coarse	2.08×10^5	0.039	-0.011	24%	40%
Medium	6.36×10^5	0.048	-0.017	6%	10%
Fine	21.8×10^5	0.051	-0.018	-	-

Table 5
Linear finite element mesh sensitivity analysis input and results for STAR-CCM+.

Mesh type	Number of degrees of freedom	Displacement normal to the plate convex surface (mm)		Relative difference from the fine mesh solution	
		Maximum	Minimum	Maximum	Minimum
Coarse	1.89×10^5	0.058	-0.022	5%	6%
Medium	6.27×10^5	0.060	-0.023	1%	2%
Fine	21.7×10^5	0.061	-0.024	-	-

Table 6
Quadratic finite element mesh sensitivity analysis input and results for COMSOL.

Mesh type	Number of degrees of freedom	Displacement normal to the plate convex surface (mm)		Relative difference from the fine mesh solution	
		Maximum	Minimum	Maximum	Minimum
Coarse	2.86×10^5	0.059	-0.023	3%	1%
Medium	7.77×10^5	0.061	-0.024	0%	0%
Fine	24.8×10^5	0.061	-0.024	-	-

(a)

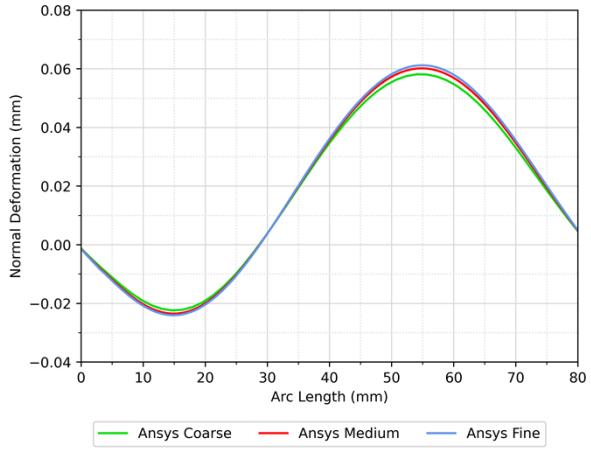

(b)

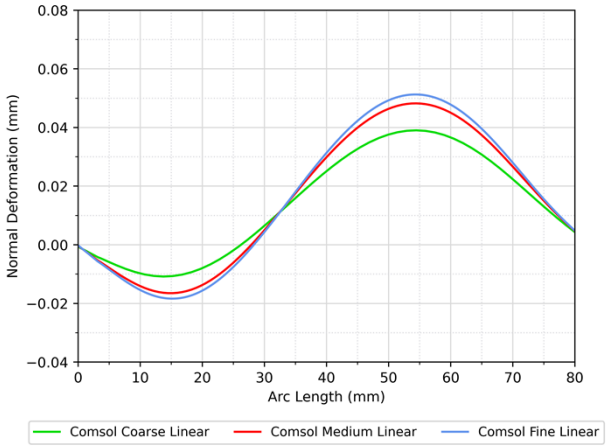

(c) (d)

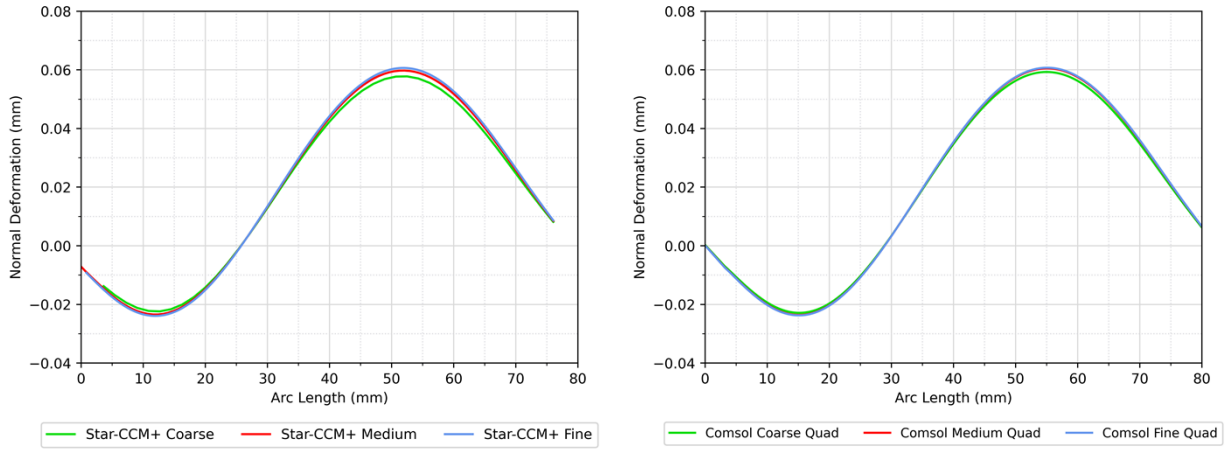

Fig. 6. Mesh sensitivity analysis in (a) ANSYS with linear, (b) COMSOL with linear, (c) STAR-CCM+ with linear, and (d) COMSOL with quadratic finite elements.

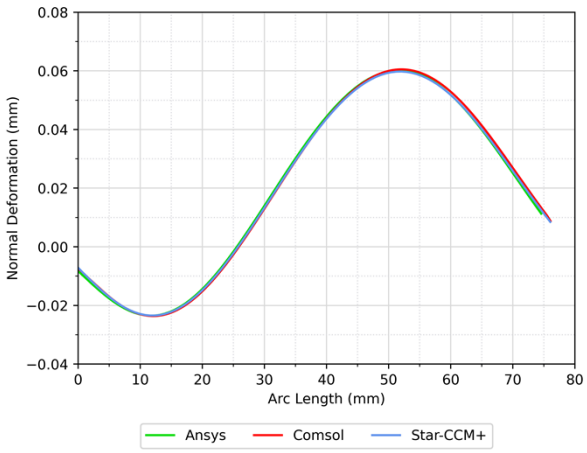

Fig. 7. Normal deformation of the mid-length obtained with the medium mesh density.

6. Simulation Results

6.1. Pressure Load

The reference case (C0) is an involute plate under a 207 kPa pressure load applied to the concave surface with the short and long edges constrained. The goal of this computation is to study the dependence of the solution on the strain-displacement relationship. The results for the reference case are shown in Fig. 8 for ANSYS, COMSOL, and STAR-CCM+. The data points are extracted at the mid-length of the involute plate. Negative displacement indicates that the involute plate deforms towards the concave side, and positive displacement means that the plate deforms to the convex side. The normal deflection is negative where the curvature radius is smaller. It becomes positive and reaches the maximum magnitude with increasing curvature radius and distance from the generating circle.

The results obtained with nonlinear geometry and the linear geometry solvers were compared. The nonlinear solver is commonly used to solve problems in which displacements are large relative to the smallest dimension of a body. Because the problems solved in this study do not exhibit large deformations, the remaining calculations are based solely on the linear solver. In the considered case, the difference

between the linear and nonlinear solutions is 11.5 % for COMSOL, 30 % for STAR-CCM+, and 12.4 % for ANSYS, with the nonlinear solver giving smaller displacements than the linear solver.

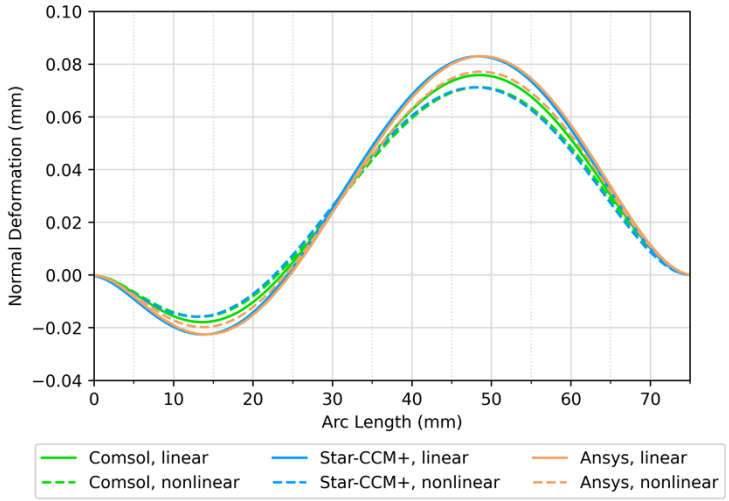

Fig. 8. Reference case results: deflection at the mid-length of the plate.

The computational and experimental mid-length deflections for Cases 1 through 4 are shown in Fig. 9. Cases 1, 2, and 3 consist of a plate with tabs measuring 6.35 mm wide with the following boundary conditions: tabs and side strips of the plate fixed (Case 1), all tabs fixed (Case 2), and every other tab fixed (Case 3). Unlike the other three cases, the tabs in Case 4 have a width of 3.175 mm. Throughout all the different scenarios, the short ends of the plate were fixed, and pressure was applied to the concave face in three stages: 69 kPa, 138 kPa, and 207 kPa. The data readings from the experiments were taken from sensors #2 (14.6 mm arc length from generating circle) and #5 (48.9 mm arc length from generating circle), capturing the deformation towards the convex and concave sides, correspondingly.

The normal displacements calculated with COMSOL, STAR-CCM+, and ANSYS in Case 1 conform remarkably well to the Cheverton–Kelley experiments with a maximum absolute difference of about 0.002 mm at 69 kPa and at 138 kPa (STAR-CCM+), and 0.037 mm at 207 kPa (ANSYS). The maximum deformation at the mid-length of the plate increases linearly with the pressure load, indicating that the deformations are elastic. Additionally, the results from the three codes compare well to each other. The largest difference between the codes is 0.0029 mm, and it occurs between Star-CCM+ and ANSYS at the final pressure load of 207 kPa. The deflection plots are presented in Fig. 9(a). The lack of constraint on the side strips of the plate induces larger normal displacements in Case 2, which is well expressed by COMSOL, STAR-CCM+, and ANSYS, as presented in Fig. 9(b). The maximum difference between the calculated values and the experimental data is 0.009 mm at 69 kPa for STAR-CCM+ and ANSYS, 0.0097 mm at 138 kPa for ANSYS, and 0.014 mm at 207 kPa for STAR-CCM+. The maximum difference between the codes is 0.0038 mm between ANSYS and STAR-CCM+ at 207 kPa.

If a weld between the involute and side plate is missing or fails, then the deformation of the plate increases. Case 3 simulates this scenario by fixing every other tab and leaving the remaining tabs unconstrained. The normal deflections at the plate mid-length are shown in Fig. 9(c) for three pressure loads. The maximum change in deflections among the codes is 0.004 mm, which is noted between ANSYS and STAR-CCM+ at 207 kPa. At 138 kPa load, COMSOL, STAR-CCM+ and ANSYS results fall in a range of 0.034 to 0.037 mm away from the experimental values. In contrast, at 207 kPa, all three codes underestimate the deflections measured in the experiment by approximately 0.15 mm. This might indicate that plastic deformations occurred for the highest load magnitude in the physical model; however, the linear elastic material model used in the analysis cannot capture this. Tab width was decreased to 3.175 mm in Case 4 to represent a scenario of narrower welds holding the fuel plate in place. In this case, more considerable

deflections are expected compared to the same set-up with 6.35 mm wide tabs in Case 2. Only the experimental deflections at sensors #2 and #5 at 138 kPa were reported in the Cheverton–Kelley report. The deformations obtained by the three codes for 138 kPa are in excellent agreement with the experimental results, with a maximum difference of 0.01 mm. Furthermore, COMSOL, STAR-CCM+, and ANSYS results compare very well, with a maximum difference of 0.017 mm between COMSOL and ANSYS.

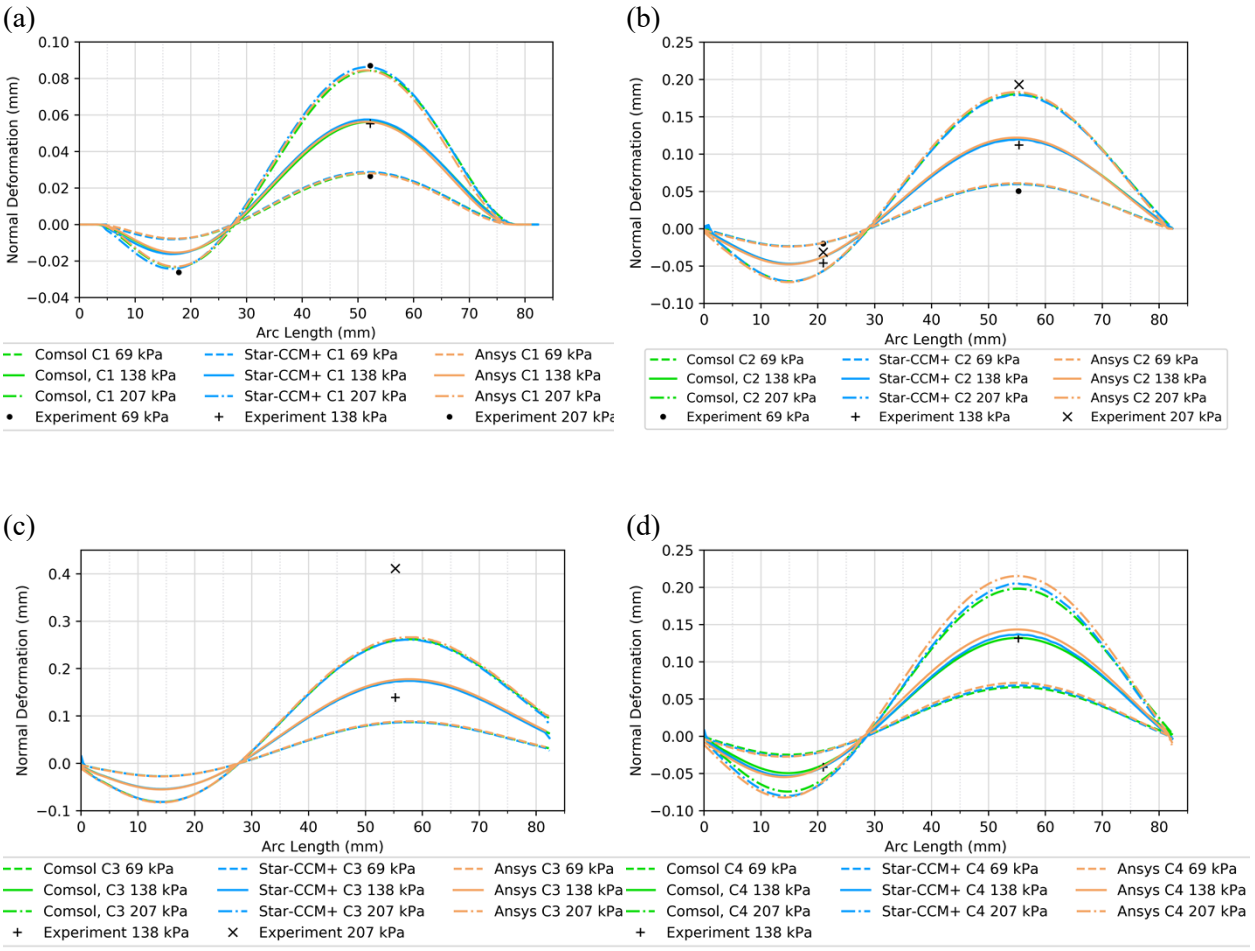

Fig. 9. Results for Cases 1–4: normal displacements of the mid-length of the fuel plate.

6.2 Temperature Load

Simulations of an involute plate under a uniform temperature load of 204 °C and an initial temperature of 27 °C were performed. The plate was mounted in a solid Invar base in this physical test. Because the thermal expansion coefficient of Invar is very low compared to other considered materials, the geometry of the base was omitted in the model. Instead, the long edges of the plate were fixed (as shown in Table 2). The normal displacements at the plate mid-length compare very well between COMSOL, STAR-CCM+, and ANSYS, as well as the experiment, as seen in Figure 10. The difference in deflections between the three codes is less than 1 %. Additionally, the computational deflections compare very well to the experimental values, with a maximum difference of approximately 0.02 mm.

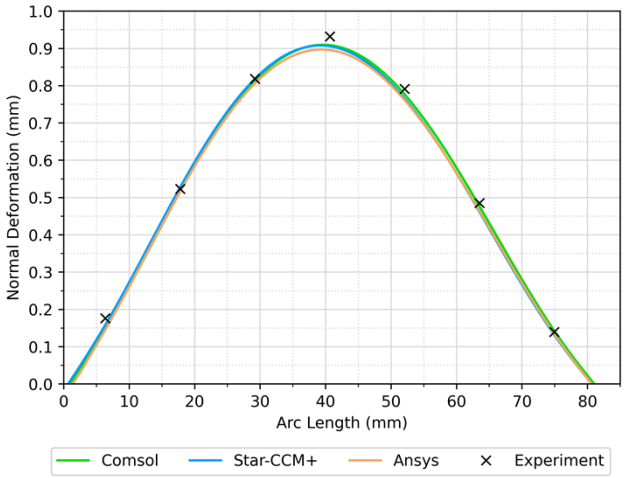

Figure 10. Case 5 results: normal displacements of the mid-length of the plate.

A more complex model consisting of the plate attached to the base was used for the remaining cases. The temperature load of 204 °C is applied uniformly to all the components. Cases 6 and 7 used a base made of Invar material in solid (Case 6) and divided (Case 7) configurations. In both cases, as shown in Table 2, a bonded contact was applied between the tabs and the base, which means that the surfaces in contact had the same displacements. The grooves and the base were in frictionless sliding contact, implying that the movement was completely limited in the normal direction, but small in-plane sliding was allowed.

Additionally, the bottom surfaces of the base are constrained in the normal direction, and the middle edge of one of the endplates is fixed to prevent rigid body motions. The results for Case 6 and Case 7 are shown in Fig. 11, which shows that the normal deformations at the plate's mid-length in the solid base configuration differ by 0.02 to 0.1 mm based on the experimental data. The differences in deformation are similar at the ends of the plate, with a difference in maximum deflection of 0.09 mm (ANSYS). The maximum difference of 0.165 mm at the plate's mid-length occurs between STAR-CCM+ and COMSOL results. The maximum difference of 0.03 mm at the ends of the plate occurs between STAR-CCM+ and ANSYS results.

The base was divided in Case 7 to account for the radial expansion of the side plates, making the deflections at the plate's mid-length smaller than in Case 6, in which the solid base was used. The exact position where the base was divided in the physical tests was not reported, so assumptions were made based on the images provided in the report.

The maximum deformations calculated by COMSOL, STAR-CCM+, and ANSYS are within ±0.22 mm from the experimental points. The shape of the short edge deflection curves is comparable to the shape obtained in the experimental data for the divided base; however, a discrepancy in the deflection profile was observed for the result obtained with COMSOL for the solid base. The minimum and maximum differences between the experiment and the codes for this location are 0.1 mm and 0.28 mm for ANSYS and COMSOL, respectively. In the code-to-code comparison, COMSOL and ANSYS have the largest difference of 0.17 mm at the plate's mid-length and 0.18 mm at the endplate.

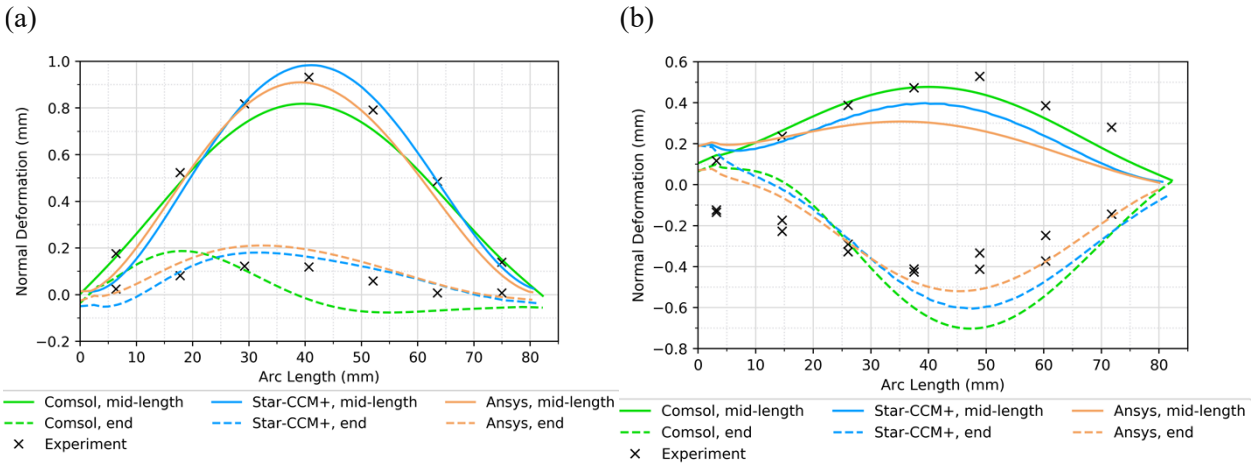

Fig. 11. Case 6 and 7 results: normal displacements of the short ends, and the mid-length of the plate mounted in (a) solid, and (b) divided base.

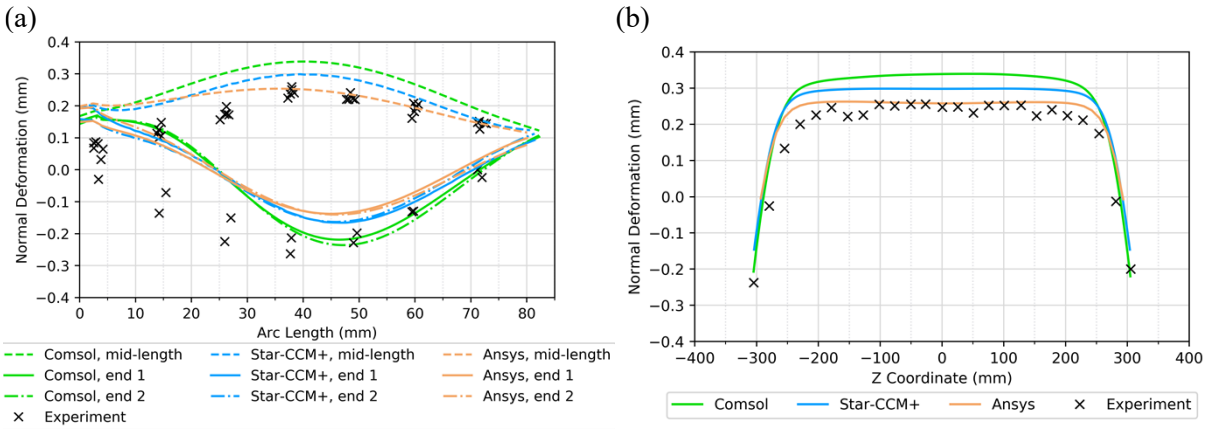

Fig. 12. Case 8 results: normal displacements of (a) the mid-length and ends of the plate, and (b) the midspan of the plate.

Case 8 consists of an aluminum plate installed in a divided steel base. The results for Case 8 are shown in Fig. 12. The normal displacements at the mid-length and at both ends of the plate are presented. All three codes managed to capture the deformation behavior quite well at the middle of the plate, with a maximum offset of approximately 0.08 mm from the experimental data. At the plate ends, the codes underestimated the deflection for the left half of the arc but represented well the deflections for the right half [see Figure 12(a)]. Despite the difference in the shape of the deflection curves, the codes predict a good agreement with the experimental data, with a maximum offset of approximately 0.09 mm. The deformation along the plate's length is presented in Figure 9(b). COMSOL, STAR-CCM+, and ANSYS results compare well to the experiment, with a maximum tolerance of 0.08 mm. The maximum difference in deflections is observed between ANSYS and COMSOL, with 0.08 mm at the plate's mid-length and 0.1 mm at the plate's end.

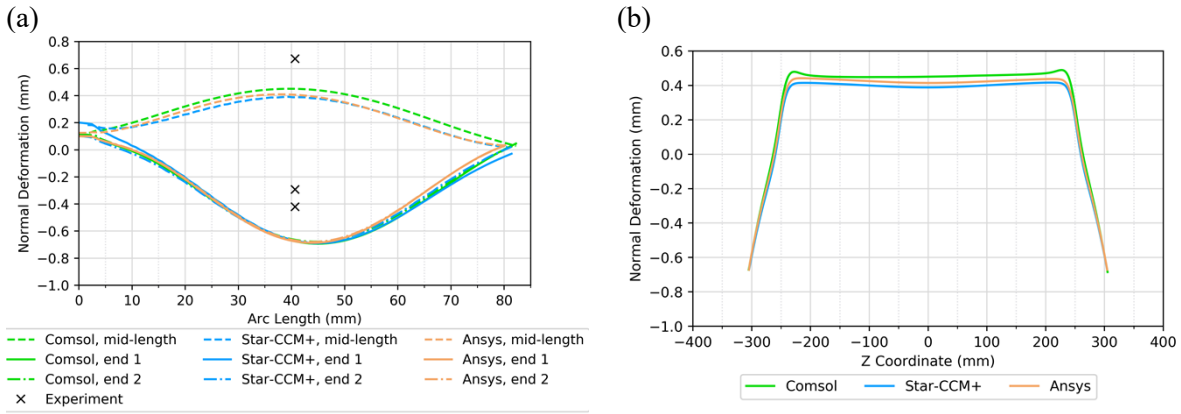

Fig. 13. Case 9 results: normal displacements of (a) the mid-length and ends of the plate, and (b) the midspan of the plate.

A HEU HFIR fuel plate has a 5 cm long unfueled section on each end, resulting in a localized abrupt temperature change where the fuel core ends. Cheverton and Kelley modeled this scenario by replacing the sections on each end of an aluminum plate model with carbon steel. Carbon steel has a lower thermal expansion coefficient compared to aluminum, allowing for modeling a discontinuous response to thermal load. The material used for the base was Invar, and the constraints were the same as in the previous cases. The Cheverton–Kelley report does not include the data readings from all seven styluses, but only the maximum and minimum deflections. Fig. 13 presents the normal displacements of (a) the mid-length and ends of the plate, and (b) the midspan of the plate. COMSOL, STAR-CCM+, and ANSYS predict deflections from 0.22 to 0.26 mm smaller than the experiment at the mid-length of the plate and almost 0.5 mm larger deflection at the end of the plate. The deflection curves along the plate length computed by the codes are very similar to each other. The effect of the cold ends can be observed in the change of the deformation shape compared to cases without cold ends, such as in Case 8. The displacements are more significant in absolute value in Case 9 than in Case 8, especially at the short ends of the plate.

6.3 Pressure and Temperature Load

In Case 10, an aluminum plate installed in a solid Monel base was tested under pressure and temperature loads. The temperature was increased from 27 to 204 °C, and the pressure load was increased from zero to 207 kPa. An essential addition to the boundary conditions, in this case, was fixing the short ends of the plate. Fig. 14 presents the normal displacements of the mid-length of the plate at 204 °C with (a) no pressure load and (b) a pressure load of 207 kPa. For the case in which the pressure load is not present, the three codes captured the shape of the deformation very well compared to the experiment, with a maximum difference of 0.08 mm. Upon applying pressure, the maximum deflection measured in the experiment increased from 0.48 to 0.52 mm. The computational results followed the same trend: the difference in maximum deflections between the experiment and calculations ranged from 0.09 to 0.12 mm.

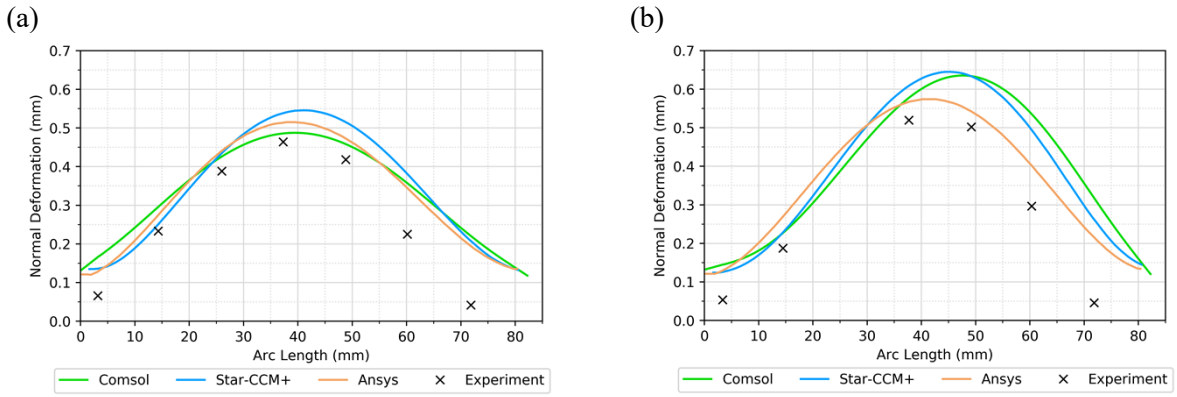

Fig. 14. Case 10 results: normal displacements of the mid-length of the plate at 204 °C with (a) no pressure load and (b) at a pressure load of 207 kPa.

7. Benchmark Case

One key objective of this paper is to propose a benchmark problem for the involute-plate–fueled research reactors based on the Cheverton–Kelley experimental findings. Table 6 lists the input parameters needed to set up the model, and Fig. 15 presents a sketch of the boundary conditions. The problem is static. The relationships between displacements and strains, as well as strains and stresses, are isotropic linear and temperature independent.

The problem was solved using a uniform finite element mesh made of eight-node hexahedral finite elements with linear shape functions and enhanced strain field in ANSYS and STAR-CCM+, and a uniform finite element mesh made of 27-node hexahedral finite elements with quadratic Lagrange shape functions in COMSOL. The ANSYS and STAR-CCM+ models were divided into 400 × 100 × 4 linear finite elements in length, span, and thickness of the plate, respectively. The COMSOL model was built with the same mesh distribution, but with quadratic Lagrange finite elements.

Table 6.
Description of the computational benchmark model.

Geometry	A 1.27 mm thick, 0.61 m long fuel plate with a cross-section based on an involute of a circle. The parametric equation of the involute is as follows: $X_{loc}(\theta) = r(\cos\theta + \theta\sin\theta)$, $Y_{loc}(\theta) = r(\sin\theta - \theta\cos\theta)$, $Z_{loc} = Z$, where $r_{in} = 149.2$ mm, and $r_{out} = 211.1$ mm. Local CSYS was created by a translation of the global CSYS by r_{in}, rotation by 180° around the X axis and 128.12° around the Z axis.
Material	Isotropic linear elastic material model with elastic modulus = 69 GPa, Poisson's ratio = 0.33, and density = 2,700 kg/m^3.
Constraints	Zero displacements on the two short and two long sides of the plate, as shown in Fig. 15.
Load	Uniform pressure load on the concave surface of the fuel plate with the magnitude of 207 kPa, as shown in Fig. 15.

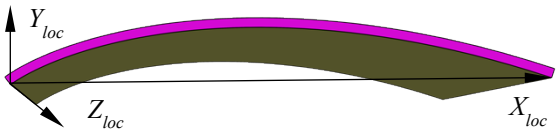

Fig. 15. Perspective view of the involute plate model in the local coordinate system (CSYS) (brown indicates pressure, and pink indicates fixed displacements).

Vertical displacements at eleven points along the mid-length curve of the convex surface were selected as the output for evaluation. The obtained values are combined in Table 7. The minimum and maximum values are the same for the three codes up to two significant digits. Some of the deflections at other locations differ in the second significant digit, and the biggest relative difference is 0.002 mm.

As a reference, an XY plot of the nodal vertical deflections obtained with STAR-CCM+ is presented in Fig. 16, and a contour plot of this field on the convex surface of the involute plate is shown in Fig. 17.

Table 7. Nodal vertical displacements of the mid-length of the convex surface of the involute.

Arc length (mm)	Nodal vertical displacement, u_y (mm)		
	ANSYS mechanical	**COMSOL multiphysics**	**Simcenter STAR-CCM+**
0.000	0.000	0.000	0.000
6.031	-0.009	-0.009	-0.009
14.137	-0.020 (min)	-0.020 (min)	-0.020 (min)
19.603	-0.014	-0.015	-0.014
26.389	0.008	0.008	0.010
33.929	0.043	0.043	0.044
41.469	0.071	0.072	0.073
48.255	0.082 (max)	0.082 (max)	0.082 (max)
55.795	0.071	0.071	0.070
63.335	0.040	0.040	0.038
74.645	0.000	0.000	0.000

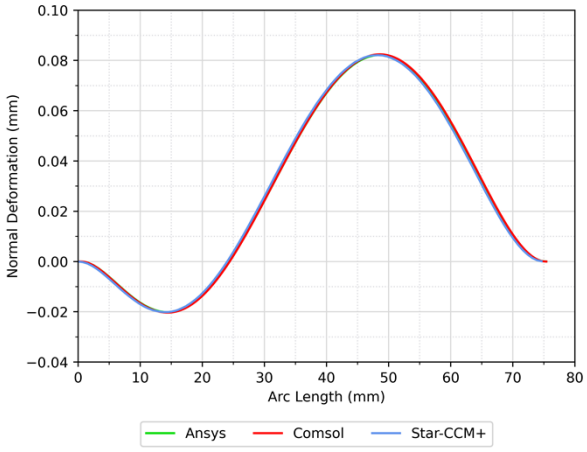

Fig. 16. Vertical deflection at the mid-length of the convex surface obtained with STAR-CCM+.

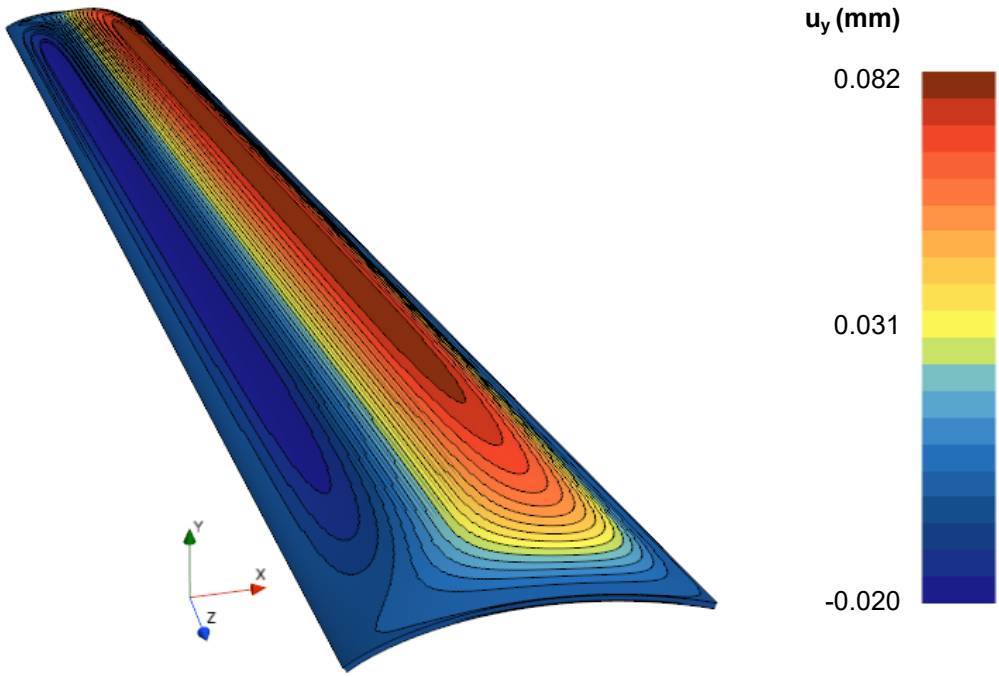

Fig. 17. Contour plot of vertical displacement of the convex surface obtained with STAR-CCM+.

8. Conclusions

Cheverton and Kelley performed a series of physical tests on a model of a single outer fuel plate from HFIR. In this study, a selected set of those experiments was modeled using FEM in three different commercial multiphysics software: ANSYS, COMSOL, and STAR-CCM+. The simulation results from the codes showed good agreement with each other and against the Cheverton–Kelley experimental data. Some minor deviations were observed for a few multiphysics cases. The possible reasons for the discrepancies may be twofold: they may have stemmed from imperfections of the experimental set-up by Cheverton and Kelley, such as from the reported non-ideal initial shape of the fuel plate in the tests, or they may have been a result of imperfections in the computational models, such as an inaccurate or overly simplified representation of the constraints or material properties. The differences in results obtained with the different codes may be related to code-specific contact interaction modeling or meshing algorithms. Overall, the modeling results were found to have significant predictive capabilities both qualitatively, as in assessing the trends for parametric variations, and quantitatively, as in magnitudes of the variables of interest, such as the normal peak deflection.

The plate deflections are reasonably accurate in the single-plate model for cases in which only elastic deformations were observed in the physical tests, such as Cases 1, 2, 4, and 5. The deformations in these cases were small compared to the coolant channel gap, which was 1.27 mm thick. For instance, the deformation caused by a 69 kPa load in Case 1 equaled approximately 0.025 mm, which is comparable to the oxide layer thickness under ANS thermal-hydraulic conditions [17]. Overall, the deflections were smaller than 1 mm. When plastic deformations occurred in the physical tests (such as in Case 3), the magnitude could not be replicated through the linear elastic material models. However, the code-to-code comparison of these cases also shows an excellent agreement.

Cases 6 to 9, representing the model of a plate in the base under thermal load, give good accuracy of deflections in the middle of the plate. The magnitude of maximum deflections differs up to 0.17 mm between the codes. Deflection curves at the mid-length of the plate have similar shapes and deflection magnitudes. The short-end deflections are more sensitive to the differences in modeling the interaction

between the plate and the base. Therefore, the deflection curves at the ends of the plate differ more significantly in shape and magnitude. The differences between the codes could result from the finite element formulations, the implementation of the contacts, and/or meshing algorithms. The average difference between the computational and experimental results is below 23 %.

An important point to note is that Cheverton and Kelley measured large deformations compared to the channel thickness of an involute reactor, namely almost 50 % of the channel thickness. However, these experiments evaluated the plate's buckling tendencies under irregular and extreme scenarios. Therefore, it is essential to conclude that ANSYS, COMSOL, and STAR-CCM+ can capture the plate behavior during different scenarios, even the non-conventional ones.

A successful code-to-code verification and experimental validation can provide the needed confidence in deploying these codes to repeat the Cheverton–Kelley tests virtually in a digital environment to evaluate new or existing designs such as the latest LEU fuel systems and plate designs, for example, low or high-density uranium silicide fuel systems and centered and symmetric fuel plate designs. A successfully validated approach makes it possible to avoid replicating an expensive thermomechanical test program for the new LEU fuel types or designs. Any new core design features, such as a longer active fuel height, or new constraints such as combs or different sizing of weld tabs, can also be investigated in more detail. Specific to HFIR, high-fidelity modeling results for the Cheverton–Kelley tests can help characterize the peak deflection profiles in the span direction that are used as an input for the steady-state margin predictions. Moreover, the Cheverton-Kelley benchmark presented in this paper was designed to improve the fidelity of predictive modeling of the involute fuel plates in an operating reactor environment. The proposed case should allow an experienced engineer to quickly set up and analyze the results. The selected solvers and models are widely available in existing CSM codes, making it possible to replicate the test. The reported minimum and maximum magnitudes of the mid-length displacements are meant to serve as reference results for evaluation.

Acknowledgments

Argonne and Oak Ridge National laboratory work were sponsored by the US Department of Energy Office of Material Management and Minimization in the US National Nuclear Security Administration Office of Defense Nuclear Nonproliferation under Contract DE-AC02-06CH11357.

Technische Universität München work was supported through a combined grant (FRM2023) from the Bundesministerium für Bildung und Forschung (BMBF) and the Bayerisches Staatsministerium für Wissenschaft und Kunst (StMWK).

The authors would also like to thank Julius Mercz for building the CAD model of the Cheverton–Kelley experimental set-up in SolidWorks.

References

[1] *High Flux Isotope Reactor – User Guide, Revision 2.0*, Oak Ridge National Laboratory, 2015.

[2] B. Jacrot, *Neutrons for Science. The Story of the First Forty Years of the Institut Laue – Langevin, Grenoble, 1967–2007, a Successful European Cooperation*. Originally published as *Des Neutrons Pour la Science*, EDP Sciences, Paris, 2006.

[3] H. Gerstenberg, I. Neuhaus, "A Brief Overview of the Research Reactor FRM II," *International Journal of Nuclear Energy Science and Technology*, vol. 4, no. 4, pp. 265–274, 2009.

[4] A. Bergeron, et al., "The Involute Working Group (IWG): Aiming at the Qualification of Advanced Computational Methods for the Conversion of Involute-Plate Reactors," 19th International Topical Meeting on Nuclear Reactor Thermal Hydraulics (NURETH-19), Brussels, Belgium, March 6–11, 2022.

[5] R. D. Cheverton, W. H. Kelley, *Experimental Investigation of HFIR Fuel Plate Deflections Induced by Temperature and Pressure Differentials*, Oak Ridge National Laboratory, ORNL-TM-2325, 1968.
[6] *ANSYS APDL Theory Reference* (www.ansys.com).
[7] *COMSOL Documentation* (www.doc.comsol.com).
[8] *Simcenter STAR-CCM+ Documentation* (www.plm.automation.siemens.com).
[9] *Standard for Verification and Validation in Computational Solid Mechanics*, ASME V&V 10-2019.
[10] R. L. Taylor, P. J. Beresford, E. L. Wilson, "A Non-Conforming Element for Stress Analysis," *International Journal for Numerical Methods in Engineering*, Vol. 10, pp.1211–1219, John Wiley & Sons, Ltd., 1976.
[11] J. C. Simo, F. Armero, "Geometrically Nonlinear Enhanced Strain Mixed Methods and the Method of Incompatible Modes," *International Journal for Numerical Methods in Engineering*, Vol. 33, pp. 1413–1449, John Wiley & Sons, Ltd., 1992.
[12] O. C. Zienkiewicz, R. L. Taylor, "The Finite Element Method for Solid and Structural Mechanics", Elsevier Butterworth-Heinemann, Oxford, sixth edition, 2006.
[13] J. C. Simo, M. S. Rifai, "A Class of Mixed Assumed Strain Methods and the Method of Incompatible Modes," *International Journal for Numerical Methods in Engineering*, Vol. 29, pp. 1595–1638, John Wiley & Sons, Ltd., 1990.
[14] *SolidWorks Documentation* (www.help.solidworks.com/).
[15] P. K. Jain, J. D. Freels, D. H. Cook, *3D COMSOL Simulations for Thermal Deflection of HFIR Fuel Plate in the "Cheverton-Kelley" Experiments*, Oak Ridge National Laboratory, ORNL/TM-2012/138, 2012.
[16] M. Sitek, A. Bergeron, C. Bojanowski, Y. Yu, J. Licht, *Involute Working Group – Development and Validation of the Finite Element Models of the Cheverton-Kelley Experiments*, Argonne National Laboratory, ANL/RTR/TM-20/15, 2020.
[17] R. E. Pawel, G. L. Yoder, C. D. West, B. H. Montgomery, *The Development of a Preliminary Correlation of Data on Oxide Growth on 6061 Aluminum Under ANS Thermal Hydraulic Conditions*, Oak Ridge National Laboratory, ORNL/TM-11517, 1990.
[18] H. A. McLain, *HFIR Fuel Element Steady State Heat Transfer Analysis*. Revised Version. United States: N. p., 1967. Web. doi:10.2172/4580058.